Available online at www.sciencedirect.com
SCIENCE DIRECT®
Journal of Solid State Chemistry 178 (2005) 742–754
JOURNAL OF SOLID STATE CHEMISTRY
www.elsevier.com/locate/jssc

X-ray powder diffraction and electron diffraction studies of the $Ni_{1\pm y}Ge_{1-x}P_x$ system

F. Javier García-García[a], A.K. Larsson[a,b,*]

[a] *Arrhenius Laboratory, Department of Inorganic Chemistry, Stockholm University, 106 91 Stockholm, Sweden*
[b] *Department of Applied Mathematics, Research School of Physical Sciences and Engineering, Australian National University, Canberra, ACT 0200, Australia*

Received 4 March 2004; received in revised form 15 October 2004; accepted 29 October 2004

Abstract

The wide-range of non-stoichiometric NiAs-type solid solution $Ni_{1\pm y}Ge_{1-x}P_x$ has been studied by means of X-ray powder and electron diffraction. The incommensurately modulated structure of Ni(Ge, P) has been found to exist over a wide compositional range which is limited by the end points $\approx NiGe_{0.8}P_{0.2}$ and $NiGe_{0.3}P_{0.7}$ so that the general stoichiometry might be referred to as $NiGe_{1-x}P_x$ with $0.2 \leqslant x \leqslant 0.7$. The modulation wave vector is of the type $\mathbf{q} = \gamma[1\,1\,\bar{2}\,0]^*$ and its modulus is strongly composition dependent. A possible interpretation is given as a "soft transition", via an incommensurately modulated structure, between the *MnP* and the *NiP* structure types, based on the almost purely displacive origin of the distortion. Further, the crystal structures of $Ni_5Ge_2P_3$ and Ni_2GeP seem to be commensurate approximations of the incommensurate modulated structure of Ni(Ge, P).

Keywords: Ni–Ge–P ternary system; Modulated NiAs-type structure; Electron diffraction; X-ray powder diffraction; Superstructure; Displacive distortion

1. Introduction

The crystal structure of the hexagonal *NiAs* structure type is frequently found among compounds formed between transition metal elements, *T*, and pinctides, chalcogenides or members of the boron or carbon groups, *B* [1,2]. The structure is simple: *T* atoms fill all the octahedral holes in a hexagonal closed packed array of *B* atoms (Figs. 1a and b). Non-stoichiometry in the transition metal sublattice is rather common and is normally accommodated in one or both of two ways. In the more intermetallic *NiAs*-type phases, the basic structure can accommodate extra *T* atoms in the trigonal bipyramidal holes of the hexagonal closed packed array and the composition is then written as $T_{2+x}B_2$. If all the trigonal bipyramids are occupied ($x = 2$), the resultant structure is of the Ni_2In type. For the more ionic phases, Ni vacancies are distributed in every second octahedral layer along the hexagonal axis and the composition is then written as $T_{2-y}B_2$. If every second octahedral layer is empty ($y = 1$), the $Cd(OH)_2$-type structure is obtained.

This surprisingly wide compositional range has traditionally been attributed to statistically occupied T sites. However, when these systems are studied by means of electron diffraction, the description of the extended homogeneity fields as disordered becomes quite doubtful as the strong interaction of electrons with matter most often reveals long- and/or short-range order in addition to the *NiAs*-type Bragg reflections. We have therefore been re-studying some previously reported wide-range non-stoichiometry *NiAs*-type systems by

*Corresponding author. Department of Applied Mathematics, Research School of Physical Sciences and Engineering, Australian National University, Canberra, ACT 0200, Australia. Fax: +61 2 61250732.
E-mail addresses: ankie.larsson@anu.edu.au, ak1110@rsphysse.anu.edu.au (A.K. Larsson).

0022-4596/$ - see front matter © 2004 Elsevier Inc. All rights reserved.
doi:10.1016/j.jssc.2004.10.040

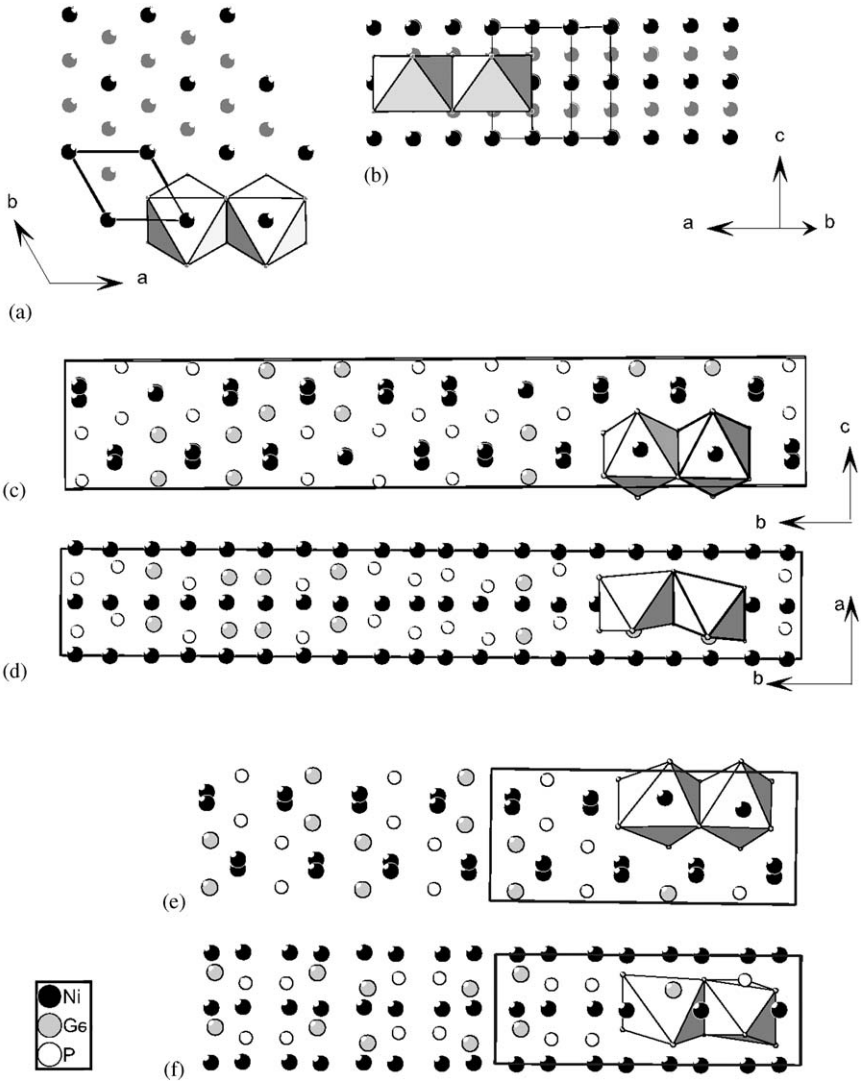

Fig. 1. In (a) and (b) the *NiAs*-type structure is sketched. Black and gray spheres represent T and B atoms, respectively. The crystal structures of $Ni_5Ge_2P_3$ (c, d) and Ni_2GeP (e, f) are shown projected down the corresponding $[0\,0\,1]_h$ and $[1\,\bar{1}\,0]_h$ directions of the basic hexagonal *NiAs*-type structure. Black, gray and white spheres represent Ni, Ge and P atoms, respectively.

means of electron diffraction. As a result new *NiAs*-type superstructures have been found, characterized and conveniently related to the previously known compounds. Examples relevant for the Ni–Ge–P system are the Ni–Ge [3] and the Co–Se [4] systems.

We have lately been expanding this study to ternary systems where the possibility of ordering between two different *B* atoms at the hexagonally close packed sites adds to the inherent complexity and offers new types of ordering patterns. In the ternary Ni–Sn–P system, a fascinating and intriguing disordered high temperature *NiAs*-type phase and three new low temperature superstructures were found [5–7]. Sn/P ordering at the *hcp* site along with ordering of extra Ni atoms into the trigonal bipyramids was confirmed as chemical reasons for the superstructures to condense out. Thus, a common structural motif could be proposed to describe the underlying crystal chemistry in this system [7].

The present study in the Ni–Ge–P system was initiated to explore the effect on the superstructural ordering when exchanging the Sn atoms in the Ni–Sn–P phases for Ge atoms. In addition to the end-member binary phases NiGe and NiP, three phases in the Ni–Ge–P system have been reported to be related to the *NiAs*-type structure: an incommensurately modulated phase [8], hereafter Ni(Ge, P), and two perfectly commensurate superstructures, $Ni_5Ge_2P_3$ [9] and Ni_2GeP [10]. Two more pseudo-binary compounds are known to exist in this system: $Ni_6(Ge, P)_3$ which is of the Ni_2P structure type [11], and $Ni(Ge, P)_2$ which is of the

FeP_2 structure type [12]. Even though their structure types deviate greatly from a *NiAs* type, it is of interest in this context to note the perfect solid solution between Ge and P in quite wide compositional ranges for these structures.

The reported crystal structures of $Ni_5Ge_2P_3$ [9] and Ni_2GeP [10] are closely related and can both be described as orthorhombic (space group *Pbca*) superstructures of a *NiAs*-type parent structure. In Figs. 1c and d, the structure of $Ni_5Ge_2P_3$ is shown projected along $[0\,0\,1]_h = [1\,0\,0]_o$ and $[1\,\bar{1}\,0]_h = [0\,0\,1]_o$, respectively (the subscript "h" here and hereafter refers to the parent hexagonal *NiAs*-type structure and "o" to refers an orthorhombic super cell). Ni_2GeP is shown in Figs. 1e and f along the corresponding directions. Both structural models can be described as Ge and P atoms defining a distorted hexagonal close packed array which has all the octahedral interstices filled with Ni. The crystallographic positions at the *hcp* array are occupied by either Ge or P atoms and no compositional disorder at these sites was reported. Displacements away from the parent structure positions are similar in both superstructures. Ni atoms are shifted out of the average T atom positions along the $[1\,\bar{1}\,0]_h$ directions so that they form zigzag chains running parallel to $[0\,0\,1]_h$ (Figs. 1c and e) while the Ge and P atoms are shifted away from the corresponding B-type position in the *NiAs*-type parent structure along $[0\,0\,1]_h$ (Figs. 1d and f).

Inspection of the reciprocal lattice of these structures shows that it is possible to describe the corresponding Bragg reflections as $\mathbf{H} = \mathbf{G} + m\mathbf{q}$, where $\mathbf{G}$ represents the parent Bragg reflections of the *NiAs*-type sublattice, $\mathbf{q} = \gamma[1\,1\,\bar{2}\,0]^*$ is a (commensurate) modulation wave vector and m is an integer. For Ni_2GeP, γ can be chosen as $3/8 = 0.375$ and for $Ni_5Ge_2P_3$, γ can be chosen as $7/20 = 0.35$.

The incommensurate displacively modulated *NiAs*-type structure reported for Ni(Ge, P) [8] was characterized by the presence of a primary modulation wave vector of the type $\mathbf{q} = (\frac{1}{3} + \delta)[1\,1\,\bar{2}\,0]^*$, with δ ranging from 0.015 to 0.019. This modulation wave vector was found to coexist with a second and perfectly commensurate modulation wave vector of the type $\mathbf{q} = \frac{1}{3}[1\,1\,\bar{2}\,0]^*$ ($\delta = 0$). A correlation between composition and the modulus of the primary modulation wave vector was not detected, and crystals with quantitatively different composition, as measured by energy dispersive X-ray spectroscopy (EDS) presented similar $\mathbf{q}$ vectors. Convergent beam electron diffraction (CBED) experiments strongly suggested a pure displacive distortion and this was additionally supported by studies based on theoretical calculation of satellite intensities [13].

Comparing the commensurate primary modulation wave vectors found for Ni_2GeP and $Ni_5Ge_2P_3$ with the primary modulation wave vector found for the incommensurate phase Ni(Ge, P), where γ was found to be in the range 0.348–0.352, reveals a striking similarity; $\gamma = 0.35$ for $Ni_5Ge_2P_3$ is exactly within the range of γ for the modulated phase and $\gamma = 0.375$ for Ni_2GeP is only slightly outside this range. This suggests that the phases are very closely related if not indeed members of the same compositionally flexible solid solution phase.

However, inspection of the reported *real space* structures brings up a clear conceptual disagreement as regards the origin of the superstructural ordering found for $Ni_5Ge_2P_3$ and Ni_2GeP compared to the incommensurately modulated structure of Ni(Ge, P). A compositional ordering of Ge and P atoms is reported to accompany the displacive modulation for the commensurate structures while a purely displacive modulation was proposed to be responsible for the structural distortion in the latter.

These contradictory results called for a re-investigation of the *NiAs*-type phase fields in the ternary system Ni–Ge–P. In particular, we aimed to determine if the commensurate phases and the modulated structure were a part of the same continuous solid solution field. If so, we aimed to determine within what range γ could be varied and if the value for γ could be related to composition. In addition, we were intrigued by reports that the incommensurate phase lacked compositional ordering while the commensurate phase was reported to have fully ordered Ge/P sites.

This contribution reports the results of a careful electron diffraction, powder X-ray diffraction and high-resolution electron microscopy (HREM) study on samples prepared along the composition line $NiGe_{1-x}P_x$ in the ternary phase diagram at 800 °C.

2. Synthesis

Samples of nominal composition $NiGe_{1-x}P_x$, $x = 0.1$, 0.2, …, 0.9, were prepared by the ceramic method. Appropriate weighed amounts of the high-purity elements were mixed together and heated up to 1000 °C for a week in sealed silica tubes. An incremental temperature rate of 100 °C a day was used. After this first treatment, the samples were then quenched to room temperature. All the samples were boulder shaped and silver colored. The specimens were homogenized in a mortar, pressed into pellets and re-annealed in closed sealed silica tubes at 800 °C for a month. The final specimens were then quenched in water to room temperature.

3. Characterization

Weak superstructural ordering along with small distortions away from the parent structure are common features of *NiAs*-type systems and hence X-ray powder

diffractograms must be treated with care. In the present case, things are additionally complicated due to the presence of incommensurately modulated structures and multiphase samples (in most samples all the phases present are modulated *NiAs*-type structures). Hence, the X-ray powder diffractograms suffer from severe overlapping of the strong parent reflections and a direct indexing of the plethora of reflections in the powder diffraction experiment is an almost impossible task. This inherent complexity can be overcome to a great extent by using electron diffraction which gives the possibility to separately study single crystals of different phases. Unit-cell dimensions, even though approximate, along with symmetry information gained in the electron microscope greatly facilitate the indexing process. Therefore, the present study is based on a combination of electron and X-ray powder diffraction.

The X-ray powder diffractograms were recorded in a Guinier–Hägg camera, using CuKα_1 radiation. Si was added as an internal standard. The films were scanned and the positions of the lines were corrected according to the internal standard. Indexing and refinement of the unit-cell parameters were carried out by least-squares using the PIRUM [14] program.

Specimens for electron microscopy were prepared by grinding the specimen under butanol and placing a drop of the resulting suspension onto a holey carbon film supported by a copper grid. Electron diffraction experiments were carried out in a JEOL 2000FX microscope operated at 200 kV. This is equipped with a LINK AN10000 analysis system which was used for EDS analysis of the crystals.

For HREM experiments, a JEM-3010 UHR microscope operating at 300 kV was used (structural resolution of 1.7 Å and Cs = 0.6 mm). For image processing of the observed experimental images, CRISP software [15] was used. The negatives were digitalized by an 8 bit video-rate CCD camera. Image simulations were carried out with the NCEMSS program system [16] using multislice algorithms.

4. Results

The resultant samples can be classified into three groups according to the phases present. In Group 1 (samples $NiGe_{0.2}P_{0.8}$ and $NiGe_{0.1}P_{0.9}$), no *NiAs*-type related structure was found and the only crystalline phases present were $Ni_2P_{1-x}Ge_x$ and $Ni_{12}(P_{1-x}Ge_x)_5$ of Ni_2P and $Ni_{12}P_5$ type, respectively. In Group 2 (samples $NiGe_{0.3}P_{0.7}$, $NiGe_{0.4}P_{0.6}$, $NiGe_{0.5}P_{0.5}$ and $NiGe_{0.6}P_{0.4}$), traces of $Ni_2P_{1-x}Ge_x$ of Ni_2P type and a modulation of a *NiAs*-type structure were the crystalline phases present while in Group 3 (samples $NiGe_{0.7}P_{0.3}$, $NiGe_{0.8}P_{0.2}$ and $NiGe_{0.9}P_{0.1}$) the crystalline phases were of $Ni_{19}Ge_{12}$ type and of *NiGe* type, and a modulation of the *NiAs*-type structure. A summary of the phases found in each sample and the refined unit-cell parameters are given in Table 1.

In addition to the crystalline phases, all samples contained varying amounts of an amorphous phase with embedded micro-crystallites. This amorphous phase consisted of a mixture of mainly germanium and phosphorus. The Ge/P ratio was very variable within each sample and no systematic change in composition was found from sample to sample. The only systematic result at this stage is that there is less of this amorphous phase in the phosphorus-rich samples. The micro-crystallites within the amorphous matrix were enriched in nickel but the size of the micro-crystallites was too small compared to the electron beam to make even a rough estimation of the composition.

In general, the Ge/P ratio of all the crystalline phases was close to the nominal Ge/P ratio of the sample. The Ni amount in the phases expressed as Ni:(Ge + P) varied from the nominal composition of 1:1 up to 2:1. The enrichment of Ni in the crystalline phases compared to the nominal composition of the samples is accounted for by the presence of the amorphous Ge/P-rich phase.

4.1. Group 1: $NiGe_{0.2}P_{0.8}$ and $NiGe_{0.1}P_{0.9}$

X-ray powder films from the sample $NiGe_{0.2}P_{0.8}$ showed only lines from a Ni_2P-type structure. For the sample $NiGe_{0.1}P_{0.9}$ some additional reflections appeared which could be indexed as belonging to a $Ni_{12}P_5$-type structure. The presence of these phases was confirmed by electron diffraction and no distortions away from these structural models were observed in the form of additional scattering. EDS analysis showed the presence of all three elements in all crystals analyzed. The highest Ge/P ratio was found in the Ni_2P-type crystals for the sample $NiGe_{0.2}P_{0.8}$ with Ni:Ge:P atomic ratios of typically ≈65:6:29, which implies ˜21% substitution of P for Ge. These observations imply the existence of a perfect solid solution with disordered Ge and P atoms arranged at the P site to 21% Ge, in agreement with earlier observations [12].

4.2. Group 2: $NiGe_{0.6}P_{0.4}$, $NiGe_{0.5}P_{0.5}$, $NiGe_{0.4}P_{0.6}$ and $NiGe_{0.3}P_{0.7}$

For these samples, all the observed reflections in the X-ray powder films could be indexed as arising either from a modulated *NiAs*-type structure or a Ni_2P-type structure. The *NiAs*-type structure was the major component in all the samples.

From the electron diffraction experiments it was clear that the *NiAs*-type reflections originated from a phase closely related to the Ni(Ge, P) phase. The main features of the reciprocal lattice of this phase can be described by Bragg reflections from the *NiAs*-type sublattice (**G**) plus

Table 1
Phases found in each sample are listed

Sample	Nominal composition	Phases found	Refined unit cell parameters
$x = 0.1$	$NiGe_{0.9}P_{0.1}$	*$Ni_{19}Ge_{12}$* NiGe Ni(Ge, P)* Ni–Ge–P_{am}	$a = 11.392(1)$, $b = 6.593(6)$, $c = 10.022(1)$, $\beta = 90.0^\circ$ $a = 5.357(1)$, $b = 3.448(1)$, $c = 5.823(3)$
$x = 0.2$	$NiGe_{0.8}P_{0.2}$	*$Ni_{19}Ge_{12}$* *NiGe* Ni(Ge, P) Ni–Ge–P_{am}	$a = 11.397(3)$, $b = 6.591(2)$, $c = 10.036(2)$, $\beta = 90.0^\circ$ $a = 5.332(1)$, $b = 3.4568(9)$, $c = 5.811(1)$
$x = 0.3$	$NiGe_{0.7}P_{0.3}$	$Ni_{19}Ge_{12}$ NiGe Ni(Ge, P) Ni–Ge–P_{am}	$a = 11.386(2)$, $b = 6.594(1)$, $c = 10.023(1)$, $\beta = 90.0^\circ$ $a = 5.312(2)$, $b = 3.4775(1)$, $c = 5.8487(3)$
$x = 0.4$	$NiGe_{0.6}P_{0.4}$	Ni(Ge, P) *Ni_2P* Ni–Ge–P_{am}	$a = 5.0417(1)$, $b = 3.4913(8)$, $c = 6.1053(1)$ $a = 5.880(1)$, $c = 3.369(2)$
$x = 0.5$	$NiGe_{0.5}P_{0.5}$	Ni(Ge, P) *Ni_2P* Ni–Ge–P_{am}	$a = 5.0099(1)$, $b = 3.4882(2)$, $c = 6.033(5)$ $a = 5.888(1)$, $c = 3.368(2)$
$x = 0.6$	$NiGe_{0.4}P_{0.6}$	Ni(Ge, P) *Ni_2P* Ni–Ge–P_{am}	$a = 4.9889(2)$, $b = 3.4615(1)$, $c = 6.0184(1)$ $a = 5.878(4)$, $c = 3.349(1)$
$x = 0.7$	$NiGe_{0.3}P_{0.7}$	Ni(Ge, P) *Ni_2P* Ni–Ge–P_{am}	$a = 4.9615(4)$, $b = 3.4616(2)$, $c = 6.027(4)$ $a = 5.880(1)$, $c = 3.369(2)$
$x = 0.8$	$NiGe_{0.2}P_{0.8}$	Ni_2P Ni–Ge–P_{am}	$a = 5.879(1)$, $c = 3.386(2)$
$x = 0.9$	$NiGe_{0.1}P_{0.9}$	*Ni_2P* $Ni_{12}P_5$ Ni–Ge–P_{am}	$a = 5.874(1)$, $c = 3.402(2)$ $a = 8.612(3)$, $c = 5.151(5)$

Note: *$Ni_{19}Ge_{12}$*, *NiGe*, *Ni_2P* and *$Ni_{12}P_5$* refer to the type structures; in these there is Ge/P substitution at the B sites corresponding roughly to the nominal composition of the sample. Ni(Ge, P) refers to the incommensurately modulated structure and Ni–Ge–P_{am} to the ternary pseudo-amorphous grains. Ni(Ge, P) crystals in the samples $x = 0.1$ were only occasionally found and are indicated by an asterisk. The refined unit cell parameters are included.

a collection of sharp and well-defined satellite reflections. All these reflections could be indexed with an expression of the type $\mathbf{H} = \mathbf{G} + m\mathbf{q}$ with $\mathbf{q} = \gamma[1\,1\,\bar{2}\,0]^*_h$ and m being an integer. The value of γ was found to be constant from grain to grain within a sample but systematically changing from sample to sample. Typical electron diffraction patterns (EDPs) from this Ni(Ge, P) phase are shown in Fig. 2. They are indexed both with respect to the parent *NiAs* structure, ''h'', and the corresponding 4D unit cell, ''o'' (see below). Figs. 2a and c are from a crystallite of the nominal $NiGe_{0.3}P_{0.7}$ sample along the zone axis $[0\,0\,1]_h = [1\,0\,0]_o$ and $[1\,\bar{1}\,0]_h = [0\,1\,0]_o$, respectively. The EDPs in Figs. 2b and d are along the same zone axes but from the nominal $NiGe_{0.5}P_{0.5}$ sample. Note that in (c) and (d) extra reflections along $[1\,1\,0]_h{}^* = [0\,0\,1]_o{}^*$ appear due to double diffraction.

The 4D, or more accurately (3 + 1)D, space group was deduced as follows: the symmetry of the sublattice is reduced to orthorhombic as the presence of the modulation destroys the initially present six-fold rotation axis. The maximal subgroup of $P6_3/mmc$ compatible with this is *Cmcm*. The setting of *Cmcm* is changed to *Amam* so that the primary modulation wave vector runs along the **c***-axis of the reciprocal cell. The reciprocal lattice unit-cell vectors are thus defined as $\mathbf{a_o}^* = -\mathbf{c_h}^*$, $\mathbf{b_o}^* = \frac{1}{2}[\bar{1}\,1\,0]^*_h$ and $\mathbf{c_o}^* = \frac{1}{2}[1\,1\,0]^*_h$. The corresponding direct space lattice vectors are given by $\mathbf{a_o} = -\mathbf{c_h}$, $\mathbf{b_o} = -\mathbf{a_h} + \mathbf{b_h}$ and $\mathbf{c_o} = \mathbf{a_h} + \mathbf{b_h}$. The reciprocal lattice can now be indexed with respect to the four reciprocal space unit-cell vectors $\mathbf{M}^* = \{\mathbf{a_o}^*, \mathbf{b_o}^*, \mathbf{c_o}^*, \mathbf{q} = \gamma\mathbf{c_o}^*\}$. The observed characteristic extinction condition becomes $F(h\,k\,l\,m) = 0$ unless $k + l = 2n$, $F(0\,k\,l\,m) = 0$ unless $k + l$ and $m = 2n$ (Figs. 2a and b) and $F(h\,0\,l\,m) = 0$ unless $h, l = 2n$ (Figs. 2c and d), with

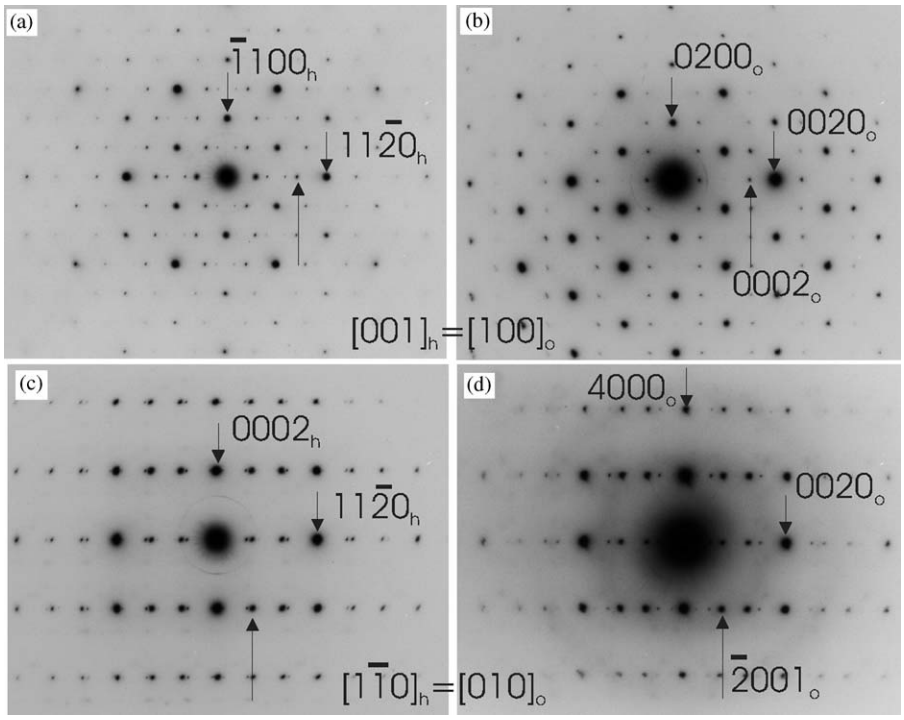

Fig. 2. In (a) and (b) typical $[0\,0\,0\,1]_h = [1\,0\,0]_o$ and in (c) and (d) typical $[\bar{1}\,1\,0\,0]_h = [0\,1\,0]_o$ zone axis EDPs. (a) and (c) are recorded in crystals from the sample $NiGe_{0.3}P_{0.7}$ (a) and (c) while (b) and (d) are recorded from the sample $NiGe_{0.5}P_{0.5}$. The indexation is with respect to both the parent hexagonal structure (subscript "h") and to the corresponding orthorhombic cell (subscript "o") of the 3 + 1D space group determined for this phase. In (b) and (d) two satellite reflections are indexed and the corresponding ones in (a) and (c) are arrowed.

h, k, l, m and n all being integers. These observed extinction conditions require the super space group to be at least $Ama2(0\,0\,\gamma)s\,0\,s$ (No. 40.4 in Table 9.8.3.5 of International Tables C [17]). The apparent *mmm* Laue symmetry however suggests $Amam(00\,\gamma)s\,0\,0$ (No. 63.6 in Table 9.8.3.5 of International Tables C [17]) as the corresponding (3 + 1)D space group.

In addition to these sharp incommensurate satellite reflections, the presence of weak and diffuse extra reflections was detected in some crystallites at $\mathbf{G}+\mathbf{q}$, where $\mathbf{q} = \langle \pm x\,0 \pm \frac{1}{3}\rangle_h^*$ with x varying, but being about 0.3–0.45. In Figs. 3a and b, EDPs along $[1\,1\,0]_h$ from crystals from the $NiGe_{0.6}P_{0.4}$ and $NiGe_{0.3}P_{0.7}$ samples, respectively, are shown. In Fig. 3c, the squared areas in (a) and (b) are shown at higher magnification to stress the presence of the extra reflections. In all the patterns in which these diffuse satellite reflections were observed, the component of $\mathbf{q}$ along $\mathbf{c_h}^*$ seemed to be locked into $\frac{1}{3}$ and the in-plane component of the modulation wave vector along $[\bar{1}\,1\,0\,0]^*$ changes between different crystals. This observation is emphasized in Fig. 3c. The intensity of this extra scattering was always rather weak but its presence was quite reproducible and found in many crystals. In spite of the strong dynamical component of electron diffraction, differences in the intensity between different crystals were inferred.

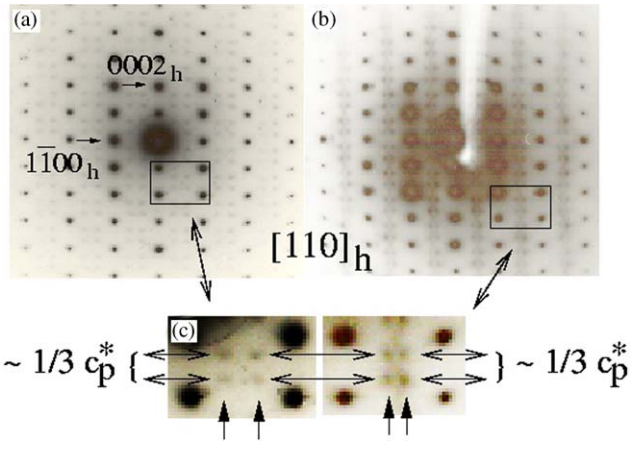

Fig. 3. In (a) and (b) two zone axes EDPs along $[1\,1\,0]_h$ from two different crystals belonging to the samples $NiGe_{0.3}P_{0.7}$ and $NiGe_{0.6}P_{0.4}$, respectively, are shown. The squared areas in these diffraction patterns are shown at higher magnification in (c) where the differences between their relatives positions are more apparent.

In an attempt to trace the origin of this extra scattering, careful EDS analyses were carried out on a number of crystals with the aim to correlate the intensity of the diffuse scattering to composition. The obtained Ge/P ratios were always in good agreement with the nominal compositions of the samples but the Ni content

was found to be quantitatively oscillating around the expected value of 50 at%. The diffraction patterns presented in Figs. 3a and b correspond to crystals with analyzed Ni contents of ≈50 and ≈48 at%, respectively. Some crystals appeared to have a Ni content well above 50 at%, but in those this extra scattering never appeared.

With only this information it is hard to work out a real space interpretation of this diffracted intensity. However, taking into account that the intensity of this scattering only seems to be present at compositions $Ni_{1-\delta}$(Ge, P) (indicating vacancies in the Ni octahedra) and that the position of these reflections are at $(x\,0\,\frac{1}{3})^*_h$ a possible interpretation turned out as feasible by recalling the reciprocal space of *NiA*s related structures in some binary systems. The reciprocal lattices of $Co_{2-x}Se_2$ [4] and $Ni_{2-x}Se_2$ [18] have been described in detail and are totally compatible with the extra scattering we observe in the Ni deficient crystallites. In $Co_{2-x}Se_2$ and $Ni_{2-x}Se_2$, the extra scattering is inferred to originate from octahedral vacancies in every second octahedral layer (along the $\mathbf{c_h}$-axis). All Ni deficient layers are identical and the ABC stacking order gives rise to the $\frac{1}{3}\mathbf{c^*}$ component. The Ni atoms in the Ni deficient layers are accommodated in hexagonal nets with a dimension *incommensurate* to the *hcp* nets. The variable dimension of the net accommodates the variable Ni content and accounts for the variation of the position of the scattered intensity perpendicular to the **c***-axis.

4.3. Group 3: $NiGe_{0.9}P_{0.1}$, $NiGe_{0.8}P_{0.2}$ and $NiGe_{0.7}P_{0.3}$

The most complicated X-ray powder films were obtained for the samples in this group. A set of *NiAs*-type Bragg reflections with the position displaced toward lower angles with respect to the Ni(Ge, P) phase found in Group 2 suggested a phase with a drastically larger *NiAs*-type subcell. In addition, sets of reflections could be indexed in a *NiGe*-type cell (or in a *Ni(Ge*, P*)*-type cell with a large orthorhombic distortion). The same type of reflection was observed for all the samples but with different relative intensity and slight shifts.

Electron diffraction experiments showed the presence of up to three different crystalline phases, all structurally related to the basic *NiAs*-type structure. This accounts for the difficulty in indexing the X-ray powder patterns. The first type of phase (accounting for the larger NiAs-type cell in the XRD patterns) is seemingly of the $Ni_{19}Ge_{12}$ type [3,19] as all observed reflections could be indexed using $\mathbf{H} = \mathbf{G} + m\mathbf{q}$, where **G** is the strong Bragg reflection from the parent *NiAs*-type structure and $\mathbf{q} = \frac{1}{6}[2\,2\,\bar{4}\,3]^*$. The compositions obtained from EDS analysis were in good agreement with this if phosphorous was allowed to replace germanium for up to 25 at%. The Ge/P ratio was in general found to be close to the Ge/P ratio of the nominal composition of the sample. Domain twinning was observed in these crystallites but the slightly more Ni-rich phases Ni_5Ge_3 and Ni_7Ge_4, with the corresponding modulation wave vectors $\mathbf{q} = \frac{1}{3}[1\,1\,\bar{2}\,2]^*$ and $\mathbf{q} = \frac{1}{4}[1\,1\,\bar{2}\,2]^*$, respectively, were never found.

EDPs of the second type of crystals found in these samples are shown in Fig. 4. In (a), (c) and (e), the $[0\,0\,1]_h$, $[1\,\bar{1}\,0]_h$ and $[1\,1\,0]_h$ zone axis patterns, respectively, are shown while in (b), (d) and (f) the EDPs after tilting the crystals a few degrees out of the corresponding zone axis conditions are shown. A careful study of these EDPs shows that all observed reflections could be indexed based on a *NiAs*-type unit cell plus a commensurate modulation wave vector of the type $\mathbf{q} = \frac{1}{2}[1\,1\,\bar{2}\,0]^*_h$. The new reciprocal unit-cell vectors might be chosen to be $\mathbf{a_o^*} = [0\,0\,\bar{1}]^*_h$, $\mathbf{b_o^*} = \frac{1}{2}[1\,1\,0]^*_h$ and $\mathbf{c_o^*} = \frac{1}{2}[1\,\bar{1}\,0]^*_h$. Thus, the corresponding real space unit-cell vectors become $\mathbf{a_o} = -\mathbf{c_h}$, $\mathbf{b_o} = \mathbf{a_h} + \mathbf{b_h}$ and $\mathbf{c_o} = \mathbf{a_h} - \mathbf{b_h}$. The observed extinctions conditions in the ED experiments are: $F(0\,k\,l) = 0$ unless $k + l =$ even (cf. Fig. 4a), $F(0\,k\,0) = 0$ unless $k =$ even and $F(0\,0\,l) = 0$ unless $l =$ even, $F(h\,k\,0) = 0$ unless $h =$ even and $F(h\,0\,0) = 0$ unless $h =$ even. The centrosymmetric space group compatible with these conditions is *Pnma* and this phase was hence identified as NiGe [20] (of the *MnP*-type structure). EDS analyses are in good agreement with this composition for that phase and phosphorous was detected in all the studied crystals in a similar amount as for the $Ni_{19}Ge_{12}$-type phase, i.e., the composition of these crystals was always similar to the nominal composition of the sample. No distortion away from the orthorhombic structure, in the form of lower symmetry or additional localized scattering of electrons, was ever observed.

Typical EDPs from the third type of phase found in these Group 3 samples are shown in Fig. 5. These crystals show an incommensurately modulated structure of the same type as that found for the *NiAs*-type crystals in the samples of Group 2. However, in the present case, some important metric distortion of the hexagonal parent structure is also observed. In (a) and (b), two zone axes EDPs from different Ni(Ge, P) crystals in the $NiGe_{0.7}P_{0.3}$ sample recorded along $[1\,\bar{1}\,0]_h$ and $[1\,\bar{1}\,1]_h$, respectively, are shown. The measured value for γ ($\approx 0.46-0.47$) agrees with the observed variation of composition (in terms of Ge/P ratio) with the modulus of the modulation wave vectors in the preceding samples. There is a discrepancy between these two EDPs as in (b) splitting of the parent reflections is clear, which is not present in (a). Note that the split reflections do not metrically correspond to the second-order satellites as seen down that direction and furthermore the observed intensity of the split reflections is much stronger than the corresponding first-order incommensurate satellites. The reflections in (b) indexed as from Ni(Ge, P) are arrowed and split reflections are

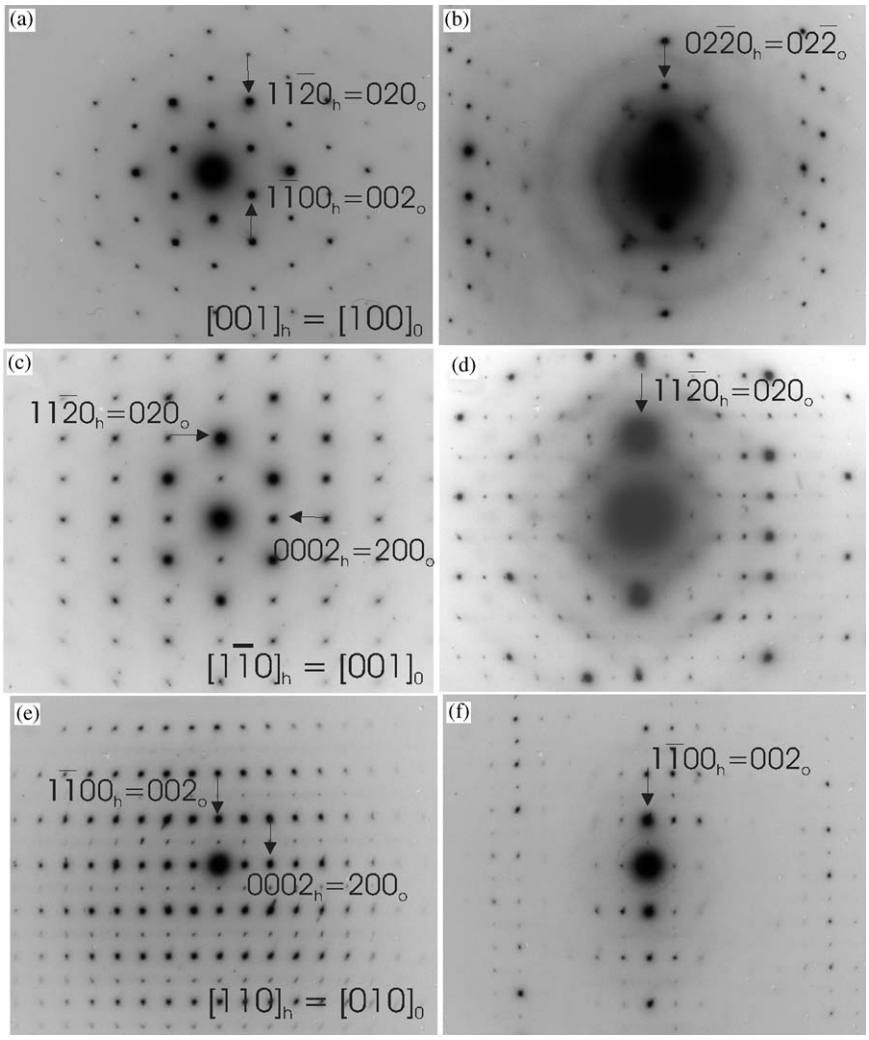

Fig. 4. Typical zone axis EDPs of the second type of crystals found in the samples of Group 3. In (a), (c) and (e) the $[0\,0\,1]_h$, $[1\,\bar{1}\,0]_h$ and $[1\,1\,0]_h$ zone axis EDPs are shown. In (b), (d) and (f) the EDPs after tilting off the crystals a few degrees out of the corresponding zone axis conditions are also presented. Note the observed extinction conditions in agreement with the *Pnma* space group of NiGe.

indicated with arrowheads. These split reflections (vide infra) were observed in the majority of the crystals as can be seen in all the following EDPs of Fig. 5.

The EDPs in Figs. 5c and d are from the sample with nominal composition $NiGe_{0.8}P_{0.2}$ along the zone axes $[1\,\bar{1}\,0]_h$ and $[1\,\bar{1}\,1]_h$, respectively. The first-order satellite reflections are visible but are noticeably weaker and less well defined than the first-order satellites observed in the sample with nominal composition $NiGe_{0.7}P_{0.3}$ (Figs. 5a and b) and no clear second-order satellites are present at all. Even though clear differences in the intensity of the satellite reflections exist between the two types of crystallites a similar value for γ (≈ 0.46) was always observed. A closer look at the EDP in Fig. 5d reveals the same splitting of the parent reflections as in Fig. 5b and also the presence of characteristic diffuse scattering. The shape of this diffuse scattering is stressed in the picture with black arcs. When looking back to the pattern in Fig. 5b, this diffuse scattering can be distinguished but in this case is more faint and blurred. To investigate the possible origin of this diffuse scattering a careful analysis of all diffraction patterns recorded was performed. Thus, a "diamond-shaped" diffuse scattering intensity distribution could be weakly detected as is discernable along $[1\,\bar{1}\,0]_h$ in Figs. 5a and c. Such a distribution of diffuse diffracted intensity is strongly reminiscent of the pattern found in *NiAs* itself [21]. Real space interpretations in that case were based on a purely displacive distortion with Ni atoms tending to form zigzag chains along the hexagonal axis of the parent structure. It is possible that similar zigzag chains are responsible for the diffuse scattering in this Ni(Ge, P) phase but due to its weakness the associated distortions are expected to be rather small.

The zone axis EDP shown in (e), along $[1\,1\,0]_h$, was also recorded in a crystal from the $NiGe_{0.8}P_{0.2}$ sample

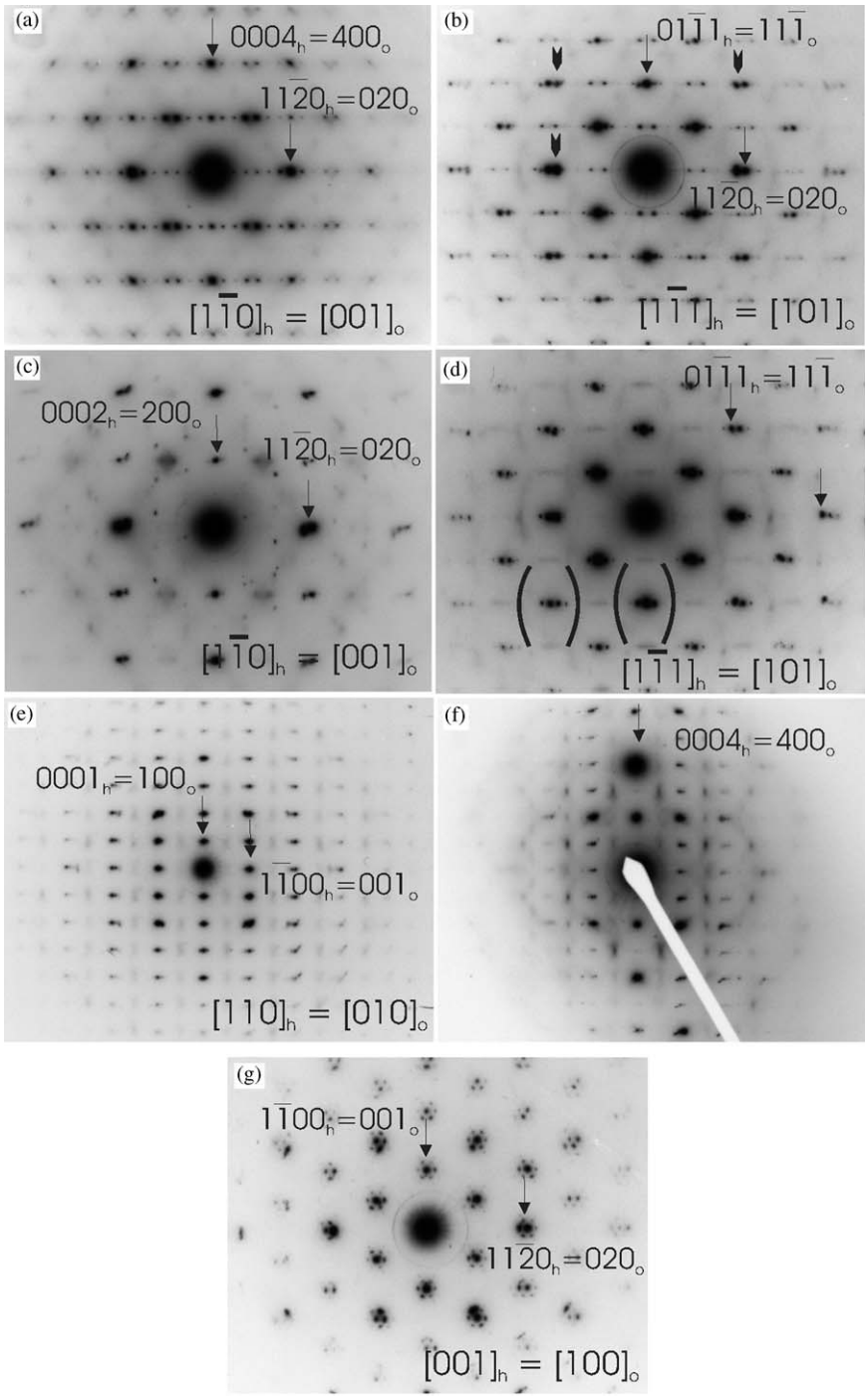

Fig. 5. The EDPs in (a) and (b) are from the sample $NiGe_{0.7}P_{0.3}$ and the rest from sample $NiGe_{0.8}P_{0.2}$. The patterns in (a) and (c) were recorded along $[1\,\bar{1}\,0]_h$ and the patterns in (b) and (d) along $[1\,\bar{1}\,1]_h$. The pattern in (e) was recorded down $[1\,1\,0]$ and in (f) the pattern when tilted slightly off this axis is shown. (g) corresponds to the $[0\,0\,1]_h$ zone axis and is obtained from the same crystal as (d). Note the presence of incommensurate modulation wave vector of the same type as observed in the patterns presented in Fig. 2 and the split main reflections in all the EDPs except in (a).

and the pattern after tilting the crystal a few degrees while keeping $[0\,0\,0\,2]_h^* = [2\,0\,0]_o^*$ excited is shown in (f). The pattern in (e) has diffuse lines of diffracted intensity running parallel to $[0\,0\,0\,1]_h^*$ seemingly condensing out at $\mathbf{q} = \frac{1}{2}[1\,\bar{1}\,0\,0]_h^*$. The tilted pattern in (f) showed that these reflections appear only or at least stronger at $(0\,0\,l)_h^*$ planes with l odd. Assuming that the corresponding $[1\,\bar{1}\,0]_h$ zone axis EDP of this crystal looks like the one presented in (c), the additional diffuse scattering present in (e) is a result of the weak and diffuse first-order satellites which are rather close to $\mathbf{q} = \frac{1}{2}[1\,1\,\bar{2}\,0]_h^*$ but not exactly at that value. Note also in (f)

the presence of the "diamond-shaped" diffuse intensity distribution mentioned above. The splitting of parent reflections is perpendicular to this zone axis but it can still be observed toward the edge of the pattern (i.e., corresponding to HOLZ).

The EDP in (g) is along $[0\,0\,1]_h$ and is recorded from the same crystal as (d). The collection of six satellites surrounding every main reflection corresponds to the splitting observed in the preceding diffraction patterns. The split reflections are invariably in the (0 0 1*) planes and there is no component along the hexagonal axis of the parent structure. At first sight, a possible interpretation of these satellites could be proposed as a result of a modulation wave vector close to $\mathbf{q} = \frac{1}{2}[1\,1\,\bar{2}\,0]^*$ (compare this EDP with those in Figs. 2a and c). This interpretation was however disregarded as the positions of the split reflections are not compatible with the satellite reflections (easiest seen in Fig. 5d). Another possibility is that it is Moirè fringes that are responsible for the reflections (vide infra).

All three samples contained these three different phases. The crystals presenting the incommensurate modulation wave vector with several orders of satellites as seen in Fig. 5a were only found in the sample $NiGe_{0.7}P_{0.3}$ while crystallites presenting the incommensurate modulation wave vector with only the first-order satellites as in Figs. 5c–g were found sometimes in the $NiGe_{0.7}P_{0.3}$ samples, were dominant in the $NiGe_{0.8}P_{0.2}$ sample and almost absent in the $NiGe_{0.9}P_{0.1}$ sample. This suggests that the ordered incommensurate structure gets rarer as the P content increases and that the crystallites with the split reflections can accommodate only small amounts of P and hence is the phase most similar to the NiGe. This similarity can also be seen by the likeness between the EDPs in Figs. 5e and f and Figs. 4e and f.

Finally, the nominal composition along with the phases found in each sample and their corresponding refined unit-cell parameters are summarized in Table 1. In Fig. 6, the X-ray powder diffractograms from the samples $NiGe_{0.7}P_{0.3}$, $NiGe_{0.4}P_{0.6}$ and $NiGe_{0.1}P_{0.9}$, respectively, are presented with the indexation of the strongest reflections indicated.

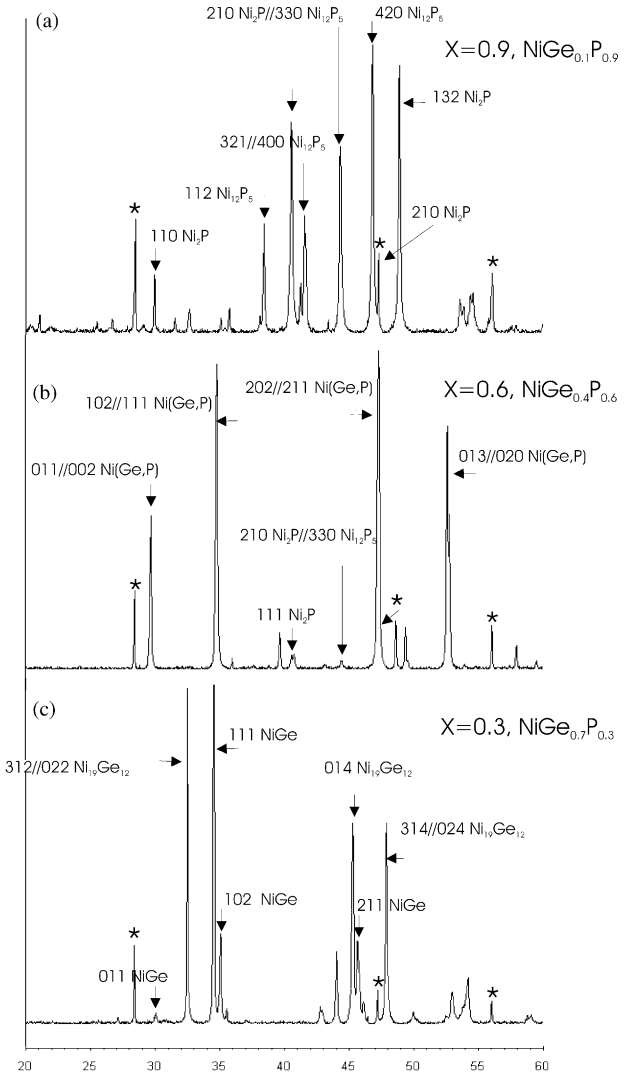

Fig. 6. X-ray powder diffractograms from the samples $x = 0.3$, 0.6 and 0.9 ($NiGe_{0.7}P_{0.3}$, $NiGe_{0.4}P_{0.6}$ and $NiGe_{0.1}P_{0.9}$, respectively) are shown. The strongest reflections are indexed.

5. High-resolution electron microscopy

In order to shed some light on the origin of the split reflections in the EDPs of the Ni(Ge, P) phase samples of Group 3, HREM experiments to image the distortions responsible for the splitting or the reflections were performed. In Fig. 7, an HREM image of a crystal from the sample $NiGe_{0.8}P_{0.2}$ oriented along the zone axis $[0\,0\,1]_h$ is shown. Black and white fringes characteristic of Moirè patterns are superimposed to the contrast from the basic hexagonal structure. Insets (a), (b) and (c) are the corresponding digital diffractograms taken in the encircled areas (a), (b) and (c), respectively. Inset (a) is indexed according to the basic hexagonal structure. No satellite reflections are present and there is no measurable deviation from a hexagonal cell. In insets (b) and (c), the basic reflections are arrowed and satellite reflections are clearly present. The black and white fringes superimposed to the basic contrast, as seen in (a), are thus responsible for the extra reflections. Filtering of areas (b) and (c) rendered the images presented in (b) and (c), respectively. Domains where the contrast is easily recognized as from the parent structure projected down the hexagonal axis are arrowed in these pictures. In (b) and (c), the inserted black and white dots, respectively, represent the periodicity observed within one of the hexagonal domains and they have been extrapolated to the neighboring domains to show that in

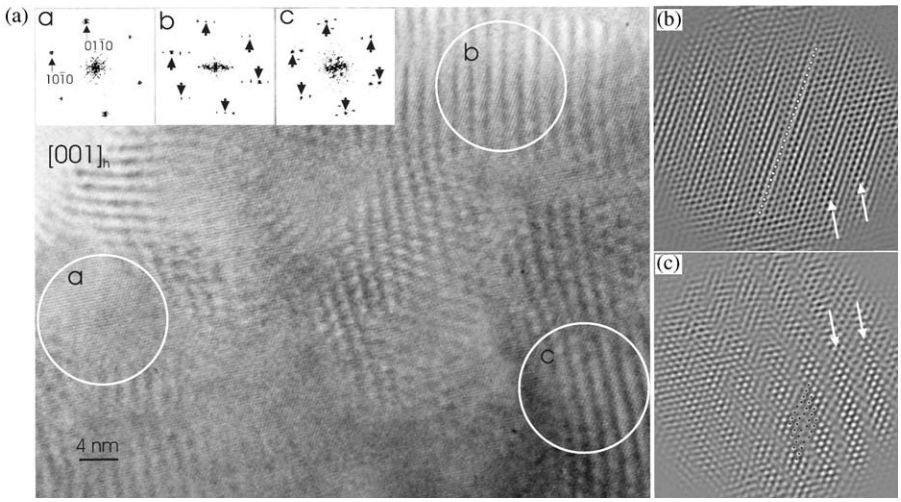

Fig. 7. HREM image of a crystals from sample $x = 0.2$ ($NiGe_{0.8}P_{0.2}$) oriented along $[0\,0\,1]_h$. Insets (a), (b) and (c) are the corresponding digital diffractograms taken in the encircled areas (a), (b) and (c), respectively. Inset (a) is indexed according to the parent hexagonal structure. In insets (b) and (c) the parent reflections from the parent structure are arrowed. Note the satellite reflections as those seen in Fig. 5 (g) as a result of the white and dark fringes observed in the corresponding areas of the image. Crystallographic filtering of areas (b) and (c) rendered the images presented in (b) and (c), respectively. Domains where the contrast is recognized as from the parent structure projected along the hexagonal axis are arrowed. In (b) and (c) the inserted black and white dots, respectively, represent the periodicity observed within the hexagonal domains. Note the presence of antiphase boundaries in (c) which cannot be seen in (b).

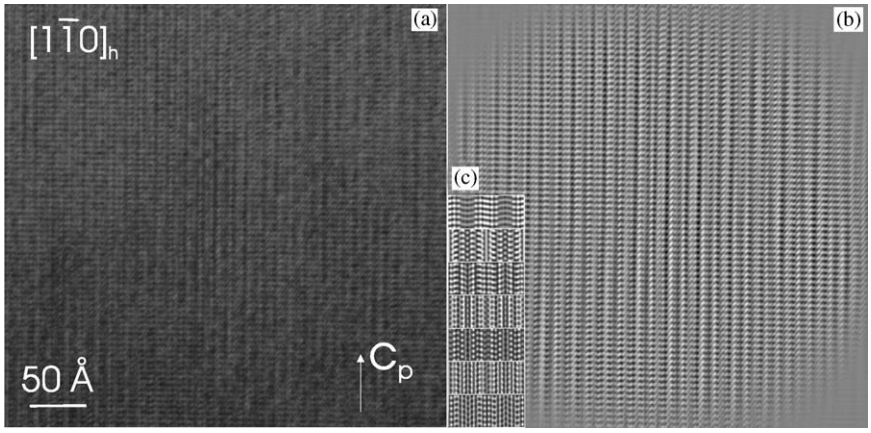

Fig. 8. In (a) an HREM image down $[1\,\bar{1}\,0]_h$ of a crystal from the sample $NiGe_{0.5}P_{0.5}$ is shown. The filtered image is presented in (b). In (c) a series of simulated high-resolution images of the crystal structure of $Ni_5Ge_2P_3$ down the corresponding direction are presented. A 10 Å thick crystal and a defocus step of −100 Å starting in the upper image for 0 Å down to −500 Å has been used. In some areas similarities between experimental and simulated images can be seen.

(c) there exist antiphase boundaries which are not observed in (b).

HREM experiments aiming to get more information on the Ni(Ge, P) structure were carried out. In Fig. 8a, an HREM image down $[1\,\bar{1}\,0]_h$ of a crystal from the sample $NiGe_{0.5}P_{0.5}$ (Group 2) is presented. The image obtained after digital filtering is shown in (b).With the attempt to check how similar the modulated structure of Ni(Ge, P) is to the commensurate approximants, a series of simulated HREM images of the crystal structure of $Ni_5Ge_2P_3$ were calculated and are shown in (c). These images were simulated for a 10 Å thick crystal and the defocus step was −100 Å starting in the upper image for 0 Å down to −500 Å. Three additional models were simulated—the first one by simply switching all P to Ge, the second one by switching all Ge to P and the third one by interchanging Ge with P atoms. The resulting simulated high-resolution images were identical to the eye in all cases, so that a possible compositional Ge/P ordering might not be detected by HREM. By comparison of the experimental and simulated images in (b) and (c), some similarities can be seen and these experiments then support that a displacive distortion of the basic structure gives rise to the modulated structure of Ni(Ge, P).

6. Discussions

All details found in the electron diffraction characterization strongly indicate that the phase we call Ni(Ge, P) corresponds to the incommensurate modulated structure of the *NiAs*-type structure previously reported [8]; compare the zone axis EDPs in Fig. 2 with those in Figs. 6 and 7 of that reference. Nevertheless, a few important differences with respect to the findings reported therein must be stressed. A second and perfectly commensurate modulation wave vector of the type $\mathbf{q} = \frac{1}{3}[1\,1\,\bar{2}\,0]^*_h$ was found to coexist with the incommensurate one in all those crystals. Such an extra modulation wave vector was never observed in our samples. The modulation wave vector $\gamma = 0.33$ found in the sample $NiGe_{0.3}P_{0.7}$ (Figs. 2a and c) is rather close but never exactly $\frac{1}{3}$ and we have seen no evidence that the modulation wave vector locks into any commensurate values. Another possibility was therefore also pondered. The monoclinic unit cell of the $Ni_{19}Ge_{12}$-type phase found in the low P content samples ($NiGe_{0.7}P_{0.3}$, $NiGe_{0.8}P_{0.2}$ and $NiGe_{0.9}P_{0.1}$) has $\mathbf{a}^* = \frac{1}{6}\mathbf{a_h}^* + \frac{1}{6}\mathbf{b_h}^*$ which along with the C centered unit cell leads to an apparent modulation wave vector of the type $\mathbf{q} = \frac{1}{3}[1\,1\,\bar{2}\,0]^*_h$. The possibility of domain intergrowth between the $Ni_{19}Ge_{12}$-type phase and Ni(Ge, P) which would give rise to this additional apparent vector $\mathbf{q} = \frac{1}{3}[1\,1\,\bar{2}\,0]^*_h$ was contemplated, but was never observed in the tilting experiments performed in the electron microscope. We could never observe $Ni_{19}Ge_{12}$-type crystals in samples with nominal composition $NiGe_{1-x}P_x$, $x \geqslant 0.4$.

The incommensurately modulated structure of Ni(Ge, P) has been found to exist over a wide compositional range which is limited by the end point $\approx NiGe_{0.8}P_{0.2}$ and $NiGe_{0.3}P_{0.7}$ so that the general stoichiometry might be referred to as $NiGe_{1-x}P_x$ with $0.2 \leqslant x \leqslant 0.7$. The modulation wave vector is strongly dependent on composition and the observed values for γ as measured in the electron diffraction experiments are presented in Table 2, along with the typical Ni:Ge:P ratios obtained. Note that in all the cases the obtained Ge/P ratio from EDS experiments have been found to coincide with the nominal composition of the samples. However, the Ni content has been found to change slightly between different crystals. Some reciprocal space details have been observed and interpreted as from modulations concerning the Ni sublattice.

In the low phosphorous content samples the crystal structure of *NiGe* type appeared and this compound is straightforwardly related to Ni(Ge, P) just by adjusting γ to $\frac{1}{2}$ along $[1\,1\,\bar{2}\,0]^*_h$. Note that a small substitution of P into these crystals was found but the electron diffraction experiments showed no corresponding distortions away from the ideal *NiGe* structure type. At the other end of the composition range, corresponding to $x = 1$, NiP is found. The crystal structure of this compound is also closely related to the *NiAs*-type so that it can be derived via a displacive commensurate modulation wave vector of the type $\mathbf{q} = \frac{1}{4}[1\,1\,\bar{2}\,0]^*_h$. Taking into account the apparent close relation between both end-member structural types, and also with the *NiAs* type, an interpretation of the modulated structure would be then made straightforwardly as a transition between these two structure types. Such an assumption is based on both the displacive character of the modulation and on the observed variation of γ with respect to composition. A quantitative analysis of the real space distortions is only possible via a full refinement of the modulated structure. We are currently working on getting diffraction data of a sufficient quality allowing further conclusions on the nature of the ordering in the modulated phase—however, small crystallites, multiphase samples and severe twinning are complicating the work.

Table 2
Nominal composition of the prepared samples, typical compositions obtained by EDS in the Ni(Ge, P) crystals and value for γ as measured in the EDPs

Nominal composition	Analyzed composition (EDS) Ni:Ge:P in atomic %	γ
$NiGe_{0.9}P_{0.1}$	≈50*:35:15	0.46*
$NiGe_{0.8}P_{0.2}$	≈50*:34:16	0.46
$NiGe_{0.7}P_{0.3}$	≈50*:35:15	0.46
$NiGe_{0.6}P_{0.4}$	≈50*:28:22	0.39
$NiGe_{0.5}P_{0.5}$	≈50*:26:24	0.37
$NiGe_{0.4}P_{0.6}$	≈50*:21:29	0.35
$NiGe_{0.3}P_{0.7}$	≈50*:17:33	0.33

Acknowledgments

This work was supported by the Swedish Research Council (VR).

References

[1] A. Kjekshus, W.B. Pearson, Prog. Solid State Chem. 1 (1964) 83.
[2] S. Lidin, A.-K. Larsson, J. Solid State Chem. 118 (1995) 313–322.
[3] A.-K. Larsson, R.L. Withers, J. Alloys Compounds 264 (1998) 125–132.
[4] L. Norèn, R.L. Withers, F.J. García-García, A.-K. Larsson, Solid State Sci. 4 (2002) 27–36.
[5] S. Furuseth, A.-K. Larsson, R.L. Withers, J. Solid State Chem. 136 (1998) 125–133.
[6] F.J. García-García, A.-K. Larsson, S. Furuseth, J. Solid State Chem. 166 (2002) 352–361.
[7] F.J. García-García, A.-K. Larsson, S. Furuseth, Solid State Sci. 6 (2004) 725–733.
[8] R. Vincent, S.F. Pretty, Philos. Mag. A 53 (6) (1973) 843–862.
[9] O.N. Il'nitskaya, Yu.B. Kuzma, Russ. J. Inorg. Chem. (Zh. Neorg. Khim.) 35 (8) (1990) 1938–1939.
[10] S.V. Orishchin, Y.B. Kuzma, Inorg. Mater. (Izv. Akad. Nauk Neorg. Mater.) 31 (3) (1995) 423–425.

[11] O.N. Il'nitskaya, Yu.B. Kuzma, Russ. J. Inorg. Chem. (Zh. Neorg. Khim.) 35 (8) (1990) 1938–1939.
[12] S.V. Orishchin, Yu.B. Kuzma, Inorg. Mater. (Izv. Akad. Nauk Neorg. Mater.) 31 (3) (1995) 423–425.
[13] R.L. Withers, D.M. Bird, J. Phys. C 19 (1986) 3507–3516.
[14] P.E. Werner, Ark. Kemi 31 (1969) 513–516.
[15] S. Hovmöller, Ultramicroscopy 41 (1992) 121.
[16] R. Kilaas, 45th Annual Proceedings of the Electron Micrsocopy Society of America, Baltimore, MD, 1987, p. 66.
[17] International Tables for Crystallography, Vol. C, 1992, p. 818.
[18] L. Norèn, V. Ting, R.L. Withers, G. Van Tendeloo, J. Solid State Chem. 161 (2001) 266–273.
[19] M. Ellner, T. Goedecke, K. Schubert, J. Less-Common Met. 24 (1971) 23–40.
[20] H. Pfisterer, K. Schubert, Z. Metallkd. 41 (1950) 358–367.
[21] G.L. Hua, T.R. Welberry, R.L. Withers, J. Phys. C 21 (1988) 3863–3876.